IEEE Photonics Journal
An IEEE Photonics Society Publication

Open Access

Deterministic Synthesis of Optical Vortices in Tailored Plasmonic Archimedes Spiral

Volume 5, Number 3, June 2013

Chen-Da Ku
Wei-Lun Huang
Jer-Shing Huang
Chen-Bin Huang

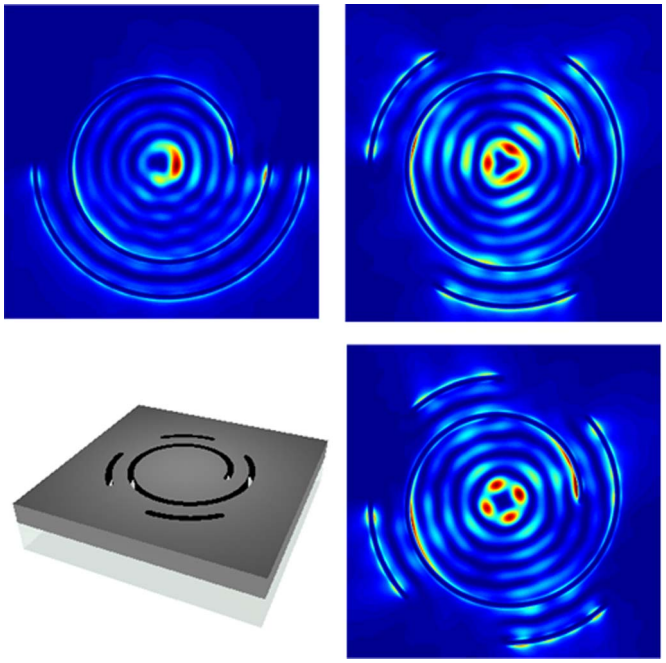

DOI: 10.1109/JPHOT.2013.2261802
1943-0655/$31.00 ©2013 IEEE

Deterministic Synthesis of Optical Vortices in Tailored Plasmonic Archimedes Spiral

Chen-Da Ku,[1] Wei-Lun Huang,[1] Jer-Shing Huang,[2,3] and Chen-Bin Huang[1]*

[1]Institute of Photonics Technologies, National Tsing Hua University, Hsinchu 30013, Taiwan
[2]Department of Chemistry, National Tsing Hua University, Hsinchu 30013, Taiwan
[3]Frontier Research Center on Fundamental and Applied Sciences of Matters, National Tsing Hua University, Hsinchu 30013, Taiwan

DOI: 10.1109/JPHOT.2013.2261802
1943-0655/$31.00 ©2013 IEEE

Manuscript received March 27, 2013; revised April 28, 2013; accepted April 30, 2013. Date of publication May 6, 2013; date of current version May 16, 2013. This work was supported in part by the National Science Council in Taiwan under Contracts NSC 100-2112-M-007-007-MY3, NSC 100-2120-M-007-007, and NSC 99-2113-M-007-020-MY2 and in part by the National Tsing Hua University in Taiwan under Grant 101N2081E1. Corresponding author: C.-B. Huang (e-mail: robin@ee.nthu.edu.tw).

Abstract: We demonstrate that the shape and the orientation of a surface plasmon (SP) vortex can be deterministically tailored through the geometrical design of a plasmonic Archimedes spiral (PAS). Noncircular SP vortices exhibiting "c," triangular, and square patterns are successfully synthesized under circular polarized plane-wave excitations. We provide clear evidence that the topological charges of the shaped SP vortices are dominated by the PAS under all geometrical settings. Our analytical description for the vortices shows excellent agreement with numerical simulations. Our design principle provides unique opportunity to manipulate nanoscale intensity and phase distribution of optical field on a flat area and may find interesting applications in plasmonic optical trapping and subwavelength patterning.

Index Terms: Surface plasmons (SPs), plasmonics, optical vortices.

1. Introduction

Surface plasmons (SPs) are waves resulting from the collective oscillations of electrons excited by electromagnetic waves at the metal/dielectric interface [1]. Such light–electron interaction provides opportunities for subwavelength spatial confinement and giant local field enhancement [2], [3]. The excitation and manipulation of SPs in designed metallic nanostructures have enabled various nanoscale devices exhibiting unique polarization sensitivities [4], [5], light-emitting capabilities [6], [7], and notably peculiar focusing effects [8], [9]. Recently, the generation of optical vortices in plasmonic systems has drawn a considerable amount of research attention. Optical vortices are waves exhibiting a phase singularity and a rotational flow around the singularity point [10]. An optical vortex is characterized by its topological charge, which denotes the number of phase singularities within a 2π azimuthal rotation. The total topological charge of a SP vortex is governed by the sum of the geometrical charge of the plasmonic structure and the angular momentum of the excitation optical beam. The generation of SP vortices has vast potentials in nanofocusing [11], [12], optical manipulations [13], and enhanced light–atom interactions [14], [15].

In [11] and [12], nanofocusing is achieved by generating zero topological charge SP vortices by exciting concentric metallic rings with radially polarized beams. Such approach requires extreme precision in geometrically aligning the illuminating beam and the metallic rings. This stringent alignment issue can be resolved for SP vortex generation in a plasmonic Archimedes spiral (PAS).

In a PAS, the optical excitation is simply a circularly polarized plane wave [16]–[19]; therefore, the alignment of the structure to a singular point of the illumination is no longer required. The direct generation of plasmonic vortex from structured illumination light or direct incident optical vortex light has been demonstrated [20]. However, in such approach, a 2-D spatial light modulator has to be used in order to generate the structured illumination beam profile. It has been shown that a PAS offers intriguing capability in generating SP vortices with controllable topological charge. In another recent study, switching between higher order SP vortices has been experimentally demonstrated using designed plasmonic slots [21]. However, in all of these remarkable works, the spatial intensity pattern of the resulting SP vortices are all azimuthally invariant, i.e., forming concentric rings.

In this paper, we numerically demonstrate that the intensity pattern of a SP vortex can be arbitrarily tailored through simple geometrical design. We demonstrate that noncircular SP vortex generations within a PAS under circularly polarized plane-wave excitation can be generated. SP vortices with intensity patterns exhibiting "c," triangular, and square shapes are successfully synthesized through the addition of designed plasmonic slots to the PAS. In addition to the control over the vortex shape, we show that the orientation of the resulting near-field SP vortex intensity distributions can also be deterministically controlled. Our numerical results are compared with analytical analyses and are all found in excellent agreements. Moreover, we provide clear evidence that the topological charge of the shaped SP vortex is dominated by the geometrical charge of the PAS. The capability in tailoring the spatial distribution of a SP vortex may find interesting applications in plasmonic-assisted optical trapping [13], [22], [23], subwavelength particle assembly [24], photoresist patterning [25], and enhanced spectroscopy [26].

2. PAS and Plasmonic Slot

In cylindrical coordinates, a PAS is formulated as $r(\phi) = r_0 + m\lambda_{spp}\phi/2\pi$, where r denotes the distance between the origin and the spiral slot, r_0 is the inner radius of the PAS, ϕ is the azimuthal angle, and λ_{spp} is the SP polariton (SPP) wavelength. Here, m defines the geometrical charge of the PAS. In this paper, we consider optical excitation of such PAS using circularly polarized plane waves carrying spin angular momentum $s = \pm 1$, where $s = 1$ and $s = -1$ denote right-hand and left-hand circularly polarized plane waves, respectively. The SP vortex field generated is mainly polarized along the z-direction and can be analytically expressed as [18]

$$\vec{E}_z(R,\phi) \propto \hat{z}\int_0^{2\pi} e^{i2\theta} e^{iRk_r\cos(\phi-\theta)}\, d\theta = \hat{z}J_q(k_{spp}R)\exp(iq\phi) \tag{1}$$

where (R,ϕ) denotes an observation point on the spiral plane, and k_{spp} is the wavenumber of the resulting SPP. J_q denotes the qth-order Bessel function of the first kind, and the corresponding order q also defines the total topological charge of the generated SP vortex. There is a simple relationship among the total topological charge, the geometrical, charge and the spin angular momentum as $q = m + s$ [27].

Our numerical analyses are performed using the 3-D finite-difference time-domain (FDTD) method [28]. The simulation volume is large enough to avoid nonphysical absorption of the near fields by the perfectly matched layers and an uniform mesh step $[(50\ \text{nm})^3]$ is used such that satisfactory calculation accuracy is obtained with reasonable speed and memory consumption. Fig. 1(a) shows the geometry of a $m = 1$ PAS, defined by $r_0 = 2400$ nm with groove width of 200 nm. In our simulations, the PAS is formed by etching through a silver film of 250-nm thickness on top of a glass substrate. The optical source is a $+$z-propagating right-hand circularly polarized $(s = 1)$ plane wave with vacuum wavelength of 1200 nm, exciting the spiral from the glass substrate. The dielectric function of silver is modeled using Drude–Lorentz function to match the experiments [29]. The dielectric function of silver at 1200 nm is given as $\varepsilon_{silver,1200nm} = -59.2 + i3.47$.

Fig. 1(b) and (c) shows the FDTD calculated z-polarized SP vortex field and phase distributions at a certain time instance, respectively. As expected, an SP vortex with total topological charge $q = 2$

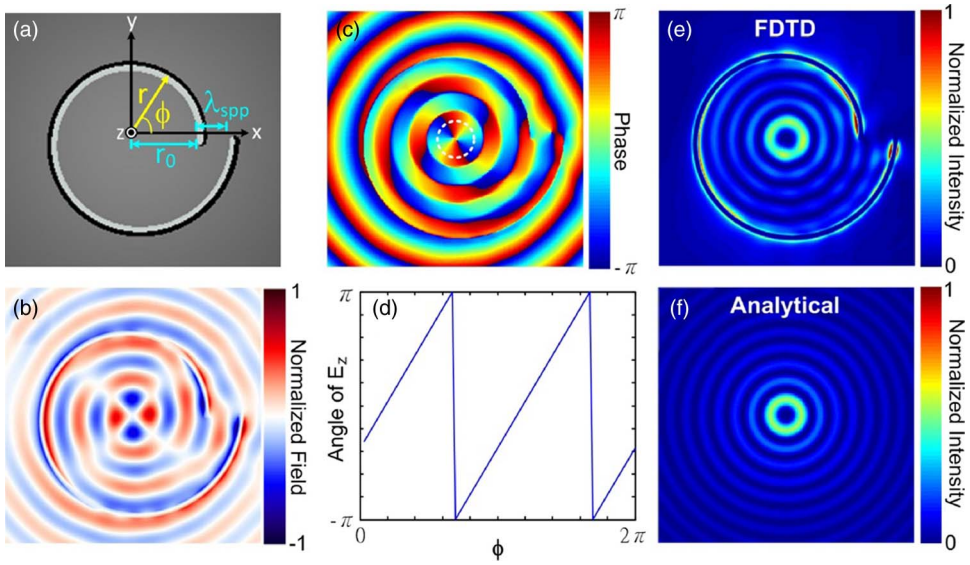

Fig. 1. (a) Geometry of the $m = 1$ PAS. (b), (c) FDTD results of instantaneous SP vortex field and phase distributions, respectively. (d) Phase profile along the dotted circle in (c). Time-averaged SP vortex intensity distributions obtained through (e) FDTD and (f) analytical calculations.

is generated: in Fig. 1(b), four field petals within a 2π azimuthal range is observed. For closer inspection over the number of phase singularities, the azimuthal line phase profile of the SPP field along the primary ring [27] [dotted circle in Fig. 1(c)] is displayed in Fig. 1(d). Fig. 1(d) reveals the phase is linear to the azimuthal angle, while two phase singularities (discontinuous phase jumps from π to $-\pi$) within a 2π range are clearly called out. Fig. 1(e) shows the time-averaged SP vortex intensity pattern, obtained through integrating the SP vortex intensities over four optical carrier cycles. The concentric rings conform to the signature of optical vortices with integer topological charge. Our FDTD result is compared with the analytical plot of $|J_2(k_{spp}R)|^2$ from (1) as depicted as Fig. 1(f) and is found in excellent agreement. We further verified that the FDTD and analytical results for the field and phase distributions are all good accords.

Fig. 2(a) shows the geometry of a plasmonic slot, defined by the same mathematical expression for a PAS, but with ϕ ranging only from 3π to 4π. Hereinafter, we refer this particular design as the π-plasmonic slot. It is interesting to learn what are the resulting SPP field, phase, and intensity distribution become as the topological charge is noninteger. Fig. 2(b) and (c) shows the z-polarized SPP field and phase distributions at a certain time instance obtained from FDTD, respectively. Our results show that the SP field and phase distributions are no longer azimuthally symmetric: the field maximum is shifted to the right of the origin, as indicated by the dashed line. The resulting SP field does not create a vortex. A movie is included as supplemental information to depict the temporal evolutions of the SP field. The azimuthal line phase profile along the dotted circle in Fig. 2(c) is displayed as Fig. 2(d), which corroborates that no phase singularity is generated. In addition to a smaller phase variation range as compared to that of a PAS, the phase increment for the π-plasmonic slot has a nonlinear dependence to the azimuthal angle. Fig. 2(e) and (f) show the FDTD and analytical time-averaged intensity patterns of the π-plasmonic slot, respectively. A tightly focused spot with lateral shift to the right of the origin is observed, suitable for nanofocusing.

3. Shaping the SP Vortex

The above analyses reveal that a plasmonic slot is capable of providing azimuthally asymmetric field components while leaving the overall SP vortex topological charge unaltered. The hybridization of a PAS and designed placements of plasmonic slots may thus enable flexible synthesis of

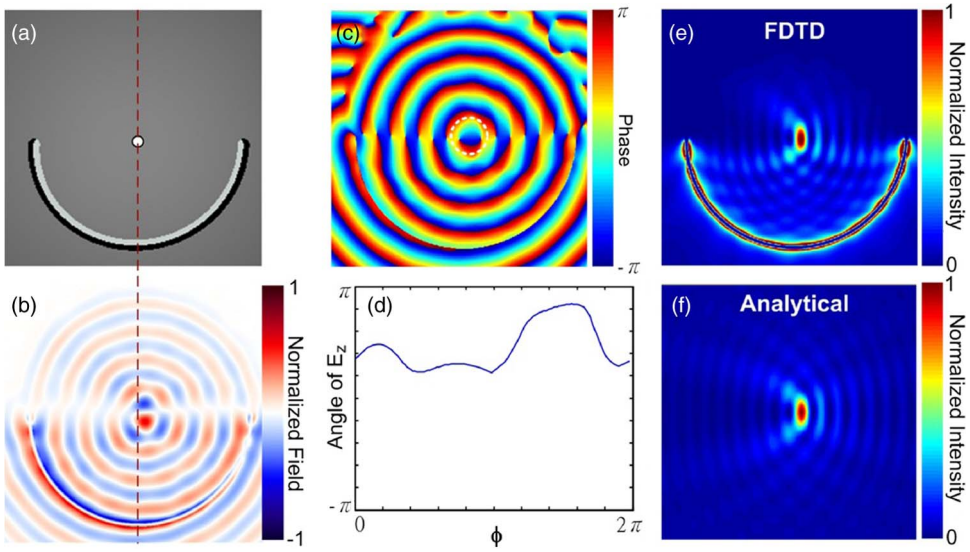

Fig. 2. (a) π-plasmonic slot. (b), (c) FDTD results of instantaneous SP field and phase distributions, respectively. (d) Phase profile along the dotted circle in (c). Time-averaged SP intensity distributions obtained through (e) FDTD and (f) analytical calculations.

deterministically shaped SP vortices. Our concept can be regarded as an extension to that reported in [21], in which only plasmonic slots were employed in creating azimuthally symmetric SP vortices.

We begin our analysis by adding a π-plasmonic slot to the $m = 1$ PAS. The geometry is shown within the inset of Fig. 3(a). The SP field can be regarded as the result of linear superposition: the main contribution from the $m = 1$ PAS, interacting coherently with the contribution from the added π-plasmonic slot. The SP vortex field for such hybridized structure is the superposition of the SPPs arising from the PAS and the added slot. Therefore, following the analogy in the derivation for (1), the SP vortex field can be analytically expressed as:

$$\vec{E}_z(R,\phi) \propto \int_0^{2\pi} e^{i2\theta} e^{iRk_r\cos(\phi-\theta)}\, d\theta + \int_{3\pi}^{4\pi} e^{i2\theta} e^{iRk_r\cos(\phi-\theta)}\, d\theta. \tag{2}$$

The instantaneous field and the instantaneous phase patterns for the hybridized structure derived from FDTD calculation are depicted in Fig. 3(a) and (b), respectively. With the addition of the π-plasmonic slot, the field and phase distributions are indeed no longer azimuthally asymmetric. The SP vortex field still exhibits four petals within a full 2π azimuth range, but notice here that, due to the broken ϕ-symmetry, the size of each petal is different and asymmetric to the origin. A movie is included as supplemental information to depict the temporal evolutions of the SP field. The phase distribution shows slight distortion in terms of the phase singularity. In order to provide closer investigations on the resulting vortex, the phase characteristics are examined using the line phase profile within the primary ring [dotted circle in Fig. 3(b)] as shown in Fig. 3(c). Clearly there are still two phase singularities within a 2π range, predominantly defined by the PAS giving a total topological charge of $q = 2$. However, the phase contribution arising from the π-plasmonic slot merely makes the phase increment slightly nonlinear to the azimuthal angle, which is the hallmark of a fractional vortex [27]. The time-averaged intensity distribution is shown in Fig. 3(d). An intensity dip in the primary ring is oriented toward the $\phi = \pi$ direction, forming an inverted "c"-shaped SP vortex pattern. The opening of the "c" points toward the left in this design. This is due to the constructive interference between the SP fields arising from the PAS and the added slot. The result

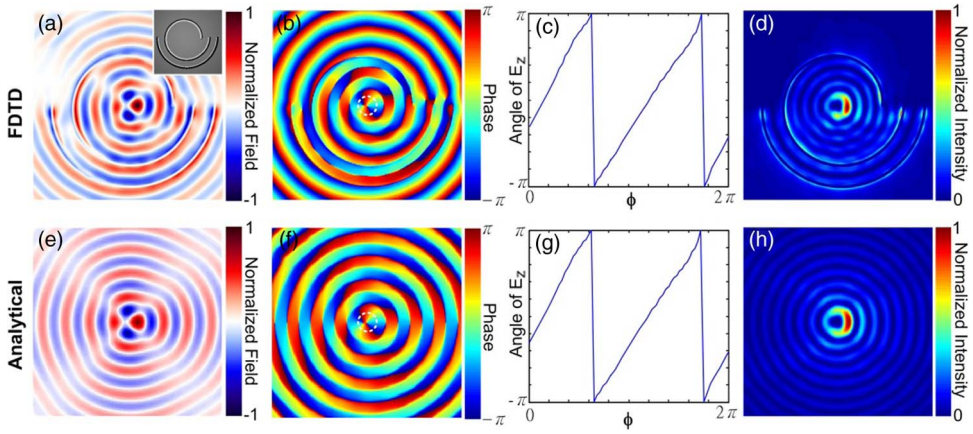

Fig. 3. FDTD results of (a) the instantaneous field, (b) the instantaneous phase, (c) the line phase profile within the primary ring, and (d) the time-averaged intensity distributions of the resulting SP vortex. The FDTD results are compared to the analytical results shown in (e)–(h).

is thus anticipated from the direct superposition of the intensity distributions shown in Figs. 1(e) and 2(e).

The analytical results for the SP vortex field, phase, line phase plot, and the time-averaged intensity distributions are shown in Fig. 3(e)–(h), respectively. Excellent agreements are observed in all comparisons between the FDTD obtained results to that derived through the analytical expression as (2). We emphasize here that, while the time-averaged intensity distribution can be arbitrarily tailored through simple geometrical design, the resulting SP vortex phase singularities of the original PAS is still retained. We demonstrate the capability in synthesizing a nonazimuthally symmetric SP vortex intensity pattern and provide the verification over the phase singularities (total topological charge) within a PAS under circularly polarized optical excitation.

The ability to control over the orientation, as well as the size of the intensity opening, is now investigated. This can be achieved through defining the total length of the added plasmonic slot. Fig. 4(a)–(c) shows the FDTD time-averaged intensity, instantaneous phase patterns, and the line phase plot when a 0.5π-plasmonic slot (defined by ϕ ranging from 2.5π to 3π) is added to the $m = 1$ PAS, respectively. The SP vortex field for this hybridized structure is analytically expressed in (3a) as

$$E_{spp}(R,\phi) = \int_{0}^{2\pi} e^{i2\theta} e^{iRk_r cos(\phi-\theta)} d\theta + \int_{2.5\pi}^{3\pi} e^{i2\theta} e^{iRk_r cos(\phi-\theta)} d\theta. \tag{3a}$$

The opening of the "c" for this design is orientated toward $\phi = \pi/4$ direction. Since the added slot length is reduce as compared with that shown in Fig. 3, the size of the intensity opening is expected to decrease in size. This anticipation is indeed confirmed in Fig. 4(a). The phase pattern shows certain distortion for the phase singularity. However, the line phase plot within the primary ring again verifies a SP vortex with two phase singularities is generated. In Fig. 4(d) and (f), the orientation of the added plasmonic slot is rotated by 90°, now being defined by ϕ ranging from 3π to 3.5π. The SP vortex field for this hybridized structure is analytically expressed in (3b) as

$$E_{spp}(R,\phi) = \int_{0}^{2\pi} e^{i2\theta} e^{iRk_r cos(\phi-\theta)} d\theta + \int_{3\pi}^{3.5\pi} e^{i2\theta} e^{iRk_r cos(\phi-\theta)} d\theta. \tag{3b}$$

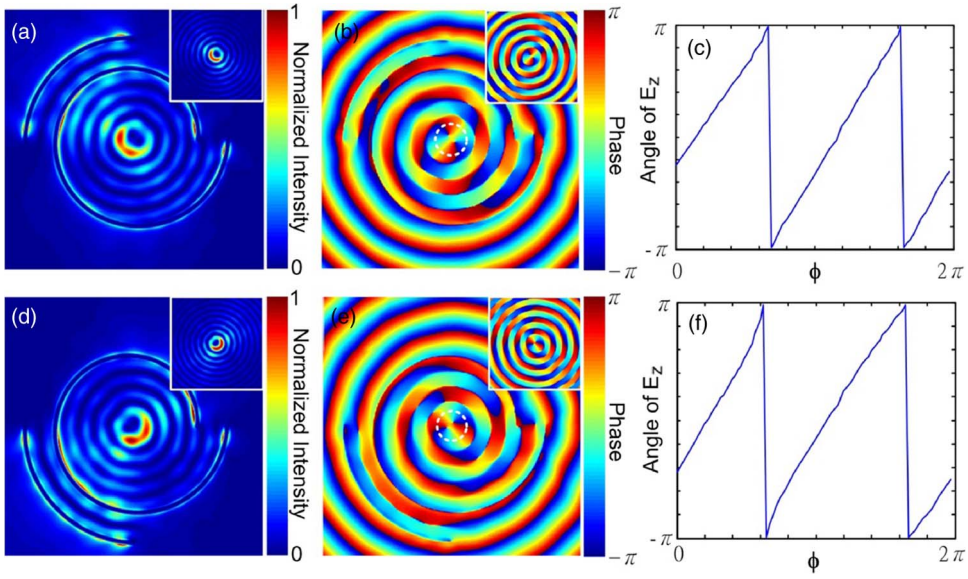

Fig. 4. Investigation on added plasmonic slot length and location. (a)–(c) Intensity, phase, and line phase plot when a slot with ϕ ranging from 2.5π to 3π is added to the PAS, respectively. (d)–(f) Plasmonic slot defined by ϕ ranging from 3π to 3.5π is added to the PAS. The analytical results are shown in the insets.

The resulting opening of the "c" is orientated toward $\phi = 3/4$ accordingly, which is completely determined by the location of the added plasmonic slot. The intensity and phase patterns derived through analytical analyses are shown as insets for both cases, showing excellent accord to the FDTD results. These examples clearly show that the orientation of the SP vortex intensity distribution can be arbitrarily tailored via simple geometrical design.

We now extend our investigation on flexible shaping of the SP vortex intensity patterns by adding multiple plasmonic slots. We demonstrate noncircular (triangular and square) SP vortex intensity distributions generated within a plasmonic spiral under circularly polarized optical excitation. In Fig. 5(a), three plasmonic slots defined by ϕ values ranging from 2π to $7\pi/3$, $8\pi/3$ to 3π, and $10\pi/3$ to $11\pi/3$ are added to the $m = 1$ PAS, respectively. The radial distance from each slot to the PAS is therefore fixed at one SPP wavelength. The SP vortex field for this hybridized structure is analytically expressed in (4a) as

$$E_{spp}(R,\phi) = \int_{0}^{\frac{7}{3}\pi} e^{i2\theta} e^{iRk_r cos(\phi-\theta)} d\theta + \int_{\frac{8}{3}\pi}^{3\pi} e^{i2\theta} e^{iRk_r cos(\phi-\theta)} d\theta + \int_{\frac{10}{3}\pi}^{\frac{11}{3}\pi} e^{i2\theta} e^{iRk_r cos(\phi-\theta)} d\theta. \quad (4a)$$

In the current hybridization, since the azimuthal angle between every two plasmonic slots is equally separated by 120°, time-averaged SP vortex intensity distribution showing an equilateral triangle is thus expected. This is indeed corroborated by the FDTD results as shown in Fig. 5(a): Three intensity peaks of equal amplitude within a full 2π rotation are generated, while the locations of these peaks are verified to be uniformly separated by 120°. The instantaneous phase pattern for such triangular SP pattern is depicted in Fig. 5(b). Although the geometrical shape of the phase is also shaped as an equilateral triangle, the line phase plot [see Fig. 5(c)] along the primary circle still exhibits two phase singularities dominated by the PAS. The corresponding intensity and phase distributions derived from analytical expressions are shown within the insets for comparison purpose. From this example, we demonstrate the potential in controlling the orientation and the geometrical shape of a triangular (isosceles or scalene) SP vortex through the design of three added plasmonic slot lengths and locations.

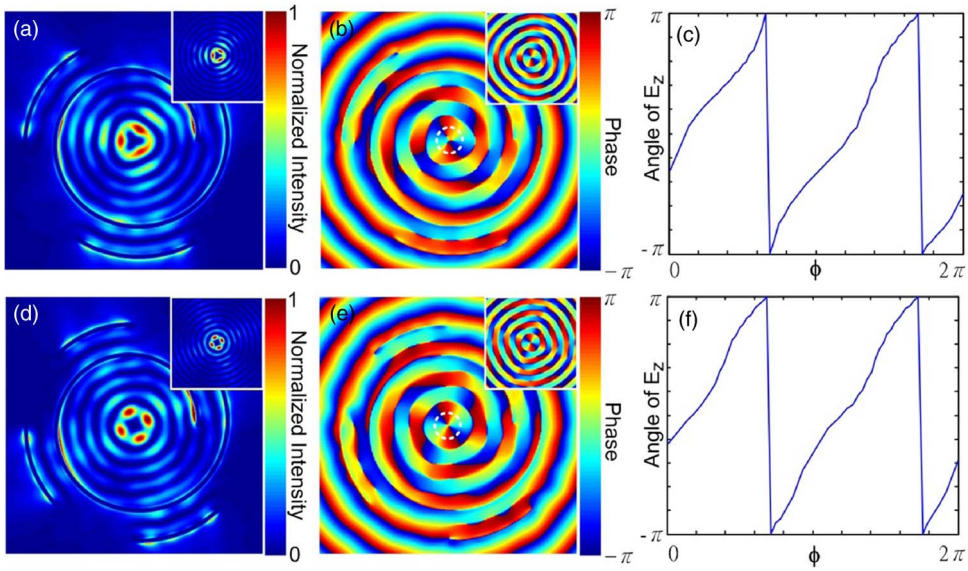

Fig. 5. Shaping the SP vortex intensity pattern using multiple added plasmonic slots. (a)–(c) Intensity, phase, and line phase plot when three plasmonic slots are added to the PAS, respectively. (d)–(f) Intensity, phase, and line phase plot when four plasmonic slots are added to the PAS, respectively. Insets: corresponding intensity and phase distributions derived from analytical expressions.

Fig. 5(d) shows the time-averaged SP vortex intensity pattern when four plasmonic slots defined by ϕ values ranging from 2π to $9\pi/4$, $5\pi/2$ to $11\pi/4$, 3π to $13\pi/4$, and $14\pi/4$ to $15\pi/4$ are added to the $m = 1$ PAS, respectively. The SP vortex field for this hybridized structure is analytically expressed in (4b) as

$$E_{spp}(R,\phi) = \int_{0}^{\frac{9}{4}\pi} e^{i2\theta} e^{iRk_r cos(\phi-\theta)}\, d\theta + \int_{\frac{5}{2}\pi}^{\frac{11}{4}\pi} e^{i2\theta} e^{iRk_r cos(\phi-\theta)}\, d\theta + \int_{3\pi}^{\frac{13}{4}\pi} e^{i2\theta} e^{iRk_r cos(\phi-\theta)}\, d\theta + \int_{\frac{14}{4}\pi}^{\frac{15}{4}\pi} e^{i2\theta} e^{iRk_r cos(\phi-\theta)}\, d\theta. \quad (4b)$$

In this design, the azimuthal angle between every two plasmonic slots is equally separated by 90°, resulting in a square shaped SP vortex intensity distribution. The instantaneous phase pattern for such square SP pattern is depicted in Fig. 5(e). Although the geometrical shape of the phase is also shaped as a square, the line phase plot [see Fig. 5(f)] along the primary circle still exhibits two phase singularities dominated by the PAS.

Close examination over the intensity distributions for the two examples shown here: with multiple added slots, we find the maxima are well aligned along with the added slots azimuthal angle. This is in contrast to the demonstrations shown in Figs. 3 and 4 (only a single added slot), where the intensity maxima are always rotated as compared to the azimuthal angle of the slot. Fig. 6 shows a comparison among the phase singularities by plotting the line phase plots of pure PAS (solid line), the example shown in Fig. 3(c) (blue dashed line), the example shown in Fig. 4(c) (green dotted line), and the example shown in Fig. 5(c) (red dash-dotted line) together. In all these designs, two well-defined phase singularities are retained. However, subtle changes in the phase increments reveal the flexibility in synthesizing a SP vortex enabled by the method outlined herein. These examples demonstrate the capabilities in arbitrary shaping the SP vortex intensity distribution, while retaining the number of SP vortex phase singularities. The line phase within the primary ring may aid the design of different vortex shapes. Our method offers possible solution to the architecture of

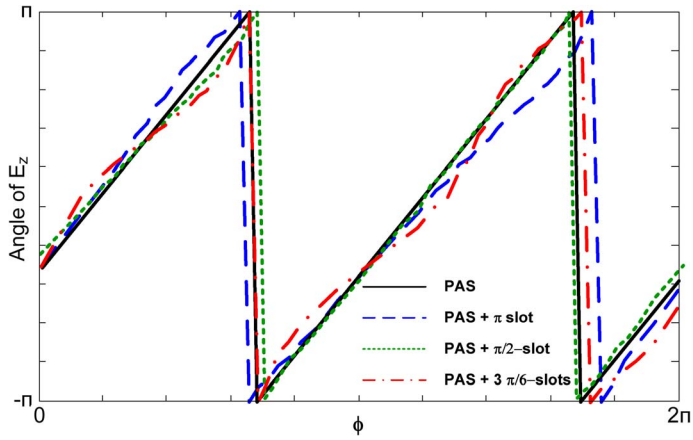

Fig. 6. Comparisons among line phase plots for various designs demonstrated.

optical near field on a planar area and facilitates applications requiring subwavelength spatiotemporal control of enhanced field. Such ability may find interesting applications in plasmonic-assisted optical trapping and enhanced spectroscopy.

4. Summary

In summary, we numerically demonstrated that the shape and orientation of a SP vortex can be arbitrarily tailored within a PAS. Through the hybridization of plasmonic slot and the PAS, SP vortices intensity shaped as "c," triangle, and square patterns are successfully synthesized. Our numerical results are compared with analytical analyses and are all found in excellent agreements. Moreover, we provide clear evidence that the number of phase singularities of the shaped SP vortices is dominated by the PAS under all geometrical settings. Our findings could find interesting applications in plasmonic-assisted optical trapping and enhanced spectroscopy, where well-defined spatial distribution of optical hot spots is required.

References

[1] S. A. Maier, *Plasmonics: Fundamentals and Applications*. New York, NY, USA: Springer-Verlag, 2007.
[2] J. A. Schuller, E. S. Barnard, W. Cai, Y. C. Jun, J. S. White, and M. L. Brongersma, "Plasmonics for extreme light concentration and manipulation," *Nat. Mater.*, vol. 9, no. 3, pp. 193–204, Mar. 2010.
[3] P. Biagioni, J.-S. Huang, and B. Hecht, "Nanoantennas for visible and infrared radiations," *Rep. Prog. Phys.*, vol. 75, no. 2, pp. 024402-1–024402-76, 2012.
[4] P. Biagioni, J.-S. Huang, L. Duò, M. Finazzi, and B. Hecht, "Cross resonant optical antenna," *Phys. Rev. Lett.*, vol. 102, no. 25, pp. 256801-1–256801-4, Jun. 2009.
[5] P.-N. Li, H.-H. Tsao, J.-S. Huang, and C.-B. Huang, "Subwavelength localization of near fields in coupled metallic spheres for single-emitter polarization analysis," *Opt. Lett.*, vol. 36, no. 12, pp. 2339–2341, Jun. 2011.
[6] N. I. Zheludev, S. L. Prosvirnin, N. Papasimakis, and V. A. Fedotov, "Lasing spaser," *Nat. Photon.*, vol. 2, no. 6, pp. 351–354, 2008.
[7] M. A. Noginov, G. Zhu, A. M. Belgrave, R. Bakker, V. M. Shalaev, E. E. Narimanov, S. Stout, E. Herz, T. Suteewong, and U. Wiesner, "Demonstration of a spaser-based nanolaser," *Nature*, vol. 460, no. 7259, pp. 1110–1113, Aug. 2009.
[8] Z. Liu, J. M. Steele, W. Srituravanich, Y. Pikus, C. Sun, and X. Zhang, "Focusing surface plasmons with a plasmonic lens," *Nano Lett.*, vol. 5, no. 9, pp. 1726–1729, Sep. 2005.
[9] S. Ishii, A. V. Kildishev, V. M. Shalaev, K.-P. Chen, and V. P. Drachev, "Metal nanoslit lenses with polarization-selective design," *Opt. Lett.*, vol. 36, no. 4, pp. 451–453, Feb. 2011.
[10] A. S. Desyatnikov, Y. S. Kivshar, and L. Torner, "Optical vortices and vortex solitons," *Prog. Opt.*, vol. 47, no. 5, pp. 291–391, 2005.
[11] G. M. Lerman, A. Yanai, and U. Levy, "Demonstration of nanofocusing by the use of plasmonic lens illuminated with radially polarized light," *Nano Lett.*, vol. 9, no. 5, pp. 2139–2143, May 2009.
[12] W. Chen, D. C. Abeysinghe, R. L. Nelson, and Q. Zhan, "Plasmonic lens made of multiple concentric metallic rings under radially polarized illumination," *Nano Lett.*, vol. 9, no. 12, pp. 4320–4325, Dec. 2009.
[13] R. Quidant and C. Girard, "Surface-plasmon-based optical manipulation," *Laser Photon. Rev.*, vol. 2, no. 1/2, pp. 47–57, Feb. 2008.

[14] V. E. Lembessis, S. Al-Awfi, M. Babiker, and D. L. Andrews, "Surface plasmon optical vortices and their influence on atoms," *J. Opt.*, vol. 13, no. 6, pp. 064002-1–064002-8, Jun. 2011.
[15] E. H. Khoo, I. Ahmed, and E. P. Li, "Manipulation of field enhancement using tapered nanobumps with circular polarization," *Appl. Phys. Lett.*, vol. 102, no. 13, pp. 131104-1–131104-5, Apr. 2013.
[16] T. Ohno and S. Miyanishi, "Study of surface plasmon chirality induced by Archimedes' spiral grooves," *Opt. Exp.*, vol. 14, no. 13, pp. 6285–6290, Jun. 2006.
[17] Y. Gorodetski, A. Niv, V. Kleiner, and E. Hasman, "Observation of the spin-based plasmonic effect in nanoscale structures," *Phys. Rev. Lett.*, vol. 101, no. 4, p. 043903, Jul. 2008.
[18] S. Yang, W. Chen, R. L. Nelson, and Q. Zhan, "Miniature circular polarization analyzer with spiral plasmonic lens," *Opt. Lett.*, vol. 34, no. 20, pp. 3047–3049, Oct. 2009.
[19] W. Chen, D. C. Abeysinghe, R. L. Nelson, and Q. Zhan, "Experimental confirmation of miniature spiral plasmonic lens as a circular polarization analyzer," *Nano Lett.*, vol. 10, no. 6, pp. 2075–2079, Jun. 2010.
[20] P. S. Tan, G. H. Yuan, Q. Wang, N. Zhang, D. H. Zhang, and X.-C. Yuan, "Phase singularity of surface plasmon polaritons generated by optical vortices," *Opt. Lett.*, vol. 36, no. 16, pp. 3287–3289, Aug. 2011.
[21] H. Kim, J. Park, S. W. Cho, S. Y. Lee, M. Kang, and B. Lee, "Synthesis and dynamic switching of surface plasmon vortices with plasmonic vortex lens," *Nano Lett.*, vol. 10, no. 2, pp. 529–536, Feb. 2010.
[22] A. N. Grigorenko, N. W. Roberts, M. R. Dickinson, and Y. Zhang, "Nanometric optical tweezers based on nanostructured substrates," *Nat. Photon.*, vol. 2, no. 6, pp. 365–370, May 2008.
[23] J.-H. Kang, K. Kim, H.-S. Ee, Y.-H. Lee, T.-Y. Yoon, M.-K. Seo, and H.-G. Park, "Low-power nano-optical vortex trapping via plasmonic diabolo nanoantennas," *Nat. Commun.*, vol. 2, no. 582, 2011.
[24] C. Renaut, J. Dellinger, B. Cluzel, T. Honegger, D. Peyrade, E. Picard, F. de Fornel, and E. Hadji, "Assembly of microparticles by optical trapping with a photonic crystal nanocavity," *Appl. Phys. Lett.*, vol. 100, no. 10, pp. 101103-1–101103-3, Mar. 2012.
[25] A. Sundaramurthy, P. James Schuck, N. R. Conley, D. P. Fromm, G. S. Kino, and W. E. Moerner, "Toward nanometer-scale optical photolithography: Utilizing the near-field of bowtie optical nanoantennas," *Nano Lett.*, vol. 6, no. 3, pp. 355–360, Mar. 2006.
[26] N. Yang, Y. Tang, and A. E. Cohen, "Spectroscopy in sculpted fields," *Nano Today*, vol. 4, no. 3, pp. 269–279, Jun. 2009.
[27] S.-W. Cho, J. Park, S.-Y. Lee, H. Kim, and B. Lee, "Coupling of spin and angular momentum of light in plasmonic vortex," *Opt. Exp.*, vol. 20, no. 9, pp. 10 083–10 094, Apr. 2012.
[28] A. F. Oskooi, D. Roundy, M. Ibanescu, P. Bermel, J. D. Joannopoulos, and S. G. Johnson, "MEEP: A flexible free-software package for electromagnetic simulations by the FDTD method," *Comput. Phys. Commun.*, vol. 181, no. 3, pp. 687–702, Mar. 2010.
[29] E. D. Palik, *Handbook of Optical Constants of Solids*. New York, NY, USA: Academic, 1985.